J Mater Sci (2010) 45:3588–3594
DOI 10.1007/s10853-010-4404-9

Moisture-cured elastomeric transparent UV and X-ray shielding organic–inorganic hybrids

C. Yang · Y. H. Tang · W. M. Lam · W. W. Lu · P. Gao · C. B. Zhao · M. M. F. Yuen

Received: 19 January 2010 / Accepted: 9 March 2010 / Published online: 23 March 2010

Abstract We report the synthesis and characterization of a kind of silane-terminated poly(ether–urethane) (PEU)-titania elastomeric hybrid for UV and X-ray shielding application. The hybrids can be easily synthesized by a moisture-cured sol–gel process at room temperature. Strong interactions between the organic and inorganic domains in these hybrids are obtained through the hydrolysis–condensation of the silane end group of the prepolymer with titanium isopropoxide (TTIP), which forms a 3D hybrid network. These hybrids exhibit adjustable mechanical properties, in a range dependent on the organic/inorganic content ratio, e.g., the hybrid containing 40 wt% of TTIP exhibits 69.3% elongation at break and excellent resilience. They show intrinsic optical transparency and the ability to completely block UV radiation in the range of UV-B and UV-A2, as well as excellent X-ray radiation blocking property. This study opens the possibility for using elastomeric coating and sealant in advanced personal protection equipments for shielding radiations.

Electronic supplementary material The online version of this article (doi:10.1007/s10853-010-4404-9) contains supplementary material, which is available to authorized users.

C. Yang (✉) · M. M. F. Yuen
Department of Mechanical Engineering, The Hong Kong University of Science and Technology, Clear Water Bay, Hong Kong, China
e-mail: yangch@ust.hk

Y. H. Tang · C. B. Zhao
Center for Advanced Marine Materials, School of Civil Engineering and Transportation, South China University of Technology, Guangzhou 510641, China

W. M. Lam · W. W. Lu
Department of Orthopaedics and Traumatology, The University of Hong Kong, Pokfulam, Hong Kong

P. Gao
Department of Mechanical Engineering, The Hong Kong University of Science and Technology, Clear Water Bay, Hong Kong, China

Introduction

Because of the growing demand for high performance materials, researchers are interested in studying functional materials and their relevant techniques. Those novel materials which can provide not only the desired functionality but also convenient processing conditions have been paid most attention [1, 2]. To this end, many interesting topics have been investigated [3–9]. In recent years, organic/inorganic hybrid materials prepared by the sol–gel approach have become a fascinating field in materials science, especially when being studied as coating materials [10, 11]. The organic/inorganic hybrid materials prepared in this way have been termed "ceramers" by Wilkes et al. [12]. Through the combinations of different inorganic and organic components in conjunction with appropriate processing methods, the hybrid materials derive benefits from the ductility of the polymer and the high Young's modulus of the ceramic as well as many other properties, [10, 13–16] such as thermal, [17–19] electrical, [20] and magnetic [21] properties for the traditional coatings. Unlike other composite materials which have much larger domain size, most of the hybrids are nanoscopic with the physical constraint of several nanometers. Therefore, these hybrids are often optically transparent.

Hybrids have various opportunities in the applied fields, such as in biomedical applications, due to their improved mechanical property and bioactivity, [22–25] and also in the personal protective clothing application for medical staff

exposed to UV and X-ray radiations, which provides them the benefit of protection due to the radiopaque and UV-blocking property of some of the ceramics [26, 27]. For the latter, the ligand-coordinated hybrids were applied as coating materials onto fabric and polymer, etc., in the optically transparent but UV-blocking and radiopaque systems [27]. Hybrids with the UV radiation shielding property have aroused a curiosity among researchers, which will significantly broaden the designing of personal radiation protective equipments, such as spacesuit and lab-coat for radioisotope user and X-ray operator in laboratories and hospitals, etc., which can provide the advantages of very little weight, stability, as well as comprehensive radiation protection [28]. Elastomeric hybrids with such kind of shielding property as well as adequate cohesive strength can be used as major parts of the radiopaque gloves and joints for airtight protective clothing to provide extraordinary comfort and safety. However, there are very few research publications about the rubbery hybrid materials which exhibit radiopaque property; [29] even though sol–gel method has been widely used as a toughening method for natural and synthetic rubbers over the past few decades [30–32].

Herein, we report our study on a kind of poly(ether-urethane) (PEU)-titania-based rubber-like hybrid material. The linear PEU prepolymer is prepared by the urethane reaction between the diethyl 2-(3-(trimethoxysilyl)propylamino)succinate and the diisocyanate terminated linear polyether (polypropylene oxide) main chain. The typical molecular weight (M_w) of the prepolymer is 43400, and polydispersity index (PDI) is 1.31. As the polyether main chain provides excellent rotational and bending ability due to the sp^3 hybridization of the C–O bond, it exhibits low Young's modulus, high flexibility, and elastomeric property. The crosslinking of the PEU pre-polymer adopts a hydrolysis and poly-condensation pathway of the two trimethoxysilane-terminated groups, which follows a general sol–gel reaction scheme [33, 34]. Because this reaction can be carried out in ambient condition, the silane-terminating pre-polymers (STPs) have demonstrated their usefulness as efficient sealing and adhering materials for automotives constructions, etc. [35, 36]. Thus, the above features make the PEUs suitable for adhering to various substrates tightly, enduring drastic deformation, and remaining cohesive to the substrate by the elastomeric nature. They also have high creep resistance due to the crosslinked structure by the trimethoxylsilyl group. As the PEU moiety has a large variety of flexible properties and excellent reliability, we are able to fabricate a hybrid coating material from a large pool of the PEU pre-polymers with appropriate properties and controllable the organic/inorganic ratio. The STPs of the PEU compound have the structure as depicted in Fig. 1a.

The end group of the STP can go through the crosslinking reaction and results in a 3D hybrid network. The

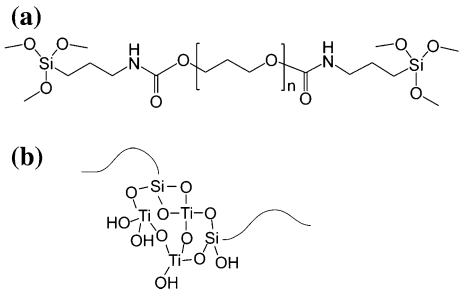

Fig. 1 **a** Structure of the silane-terminated prepolymer (STP). The linear polypropylene oxide chain contains about 750 repeating units. **b** Titania moieties involved crosslinking sites

reaction mechanism involves a two-stage process [34]. The first stage is the hydrolysis and the second stage is condensation, as described in the following (Scheme 1) [10].

As demonstrated in Scheme 1, the above process allows the silane groups react with each other and with the inorganic precursor, i.e., titanium isopropoxide (TTIP) as well, forming the ceramic island structures as demonstrated in Fig. 1b.

In this study, the co-condensation sol–gel process is carried out at room temperature in an organic solvent (dichloromethane). When the mixture is exposed to the air, the elastomeric hybrid film is formed due to solvent evaporation and moisture-induced crosslinking reaction which involves with the environmental moisture. We deal with the synthesis and characterization of the new hybrids. Mechanical property, UV- and X-ray-shielding efficiency, thermal property, and micromorphology of the hybrids are investigated in detail.

Experimental procedures

Materials

The silane-terminated prepolymer (STP) ($M_w = 43400$, PDI =1.31) (Bayermaterialscience AU, Desmoseal 2636XP), titanium tetraisopropoxide (TTIP) (Aldrich, 99%), dibutyl tin dilaurate (Aldrich, 99%), and dichloromethane (Aldrich, AR) were used as received.

Preparations

The synthesis of hybrid H-50 is described as an example: 4.0 g of TTIP is added to 6.0 g of dichloromethane (solution 1). In a separate container 4.0 g of STP is dissolved in 6.0 g of dichloromethane (solution 2). After completion of the prepolymer dissolution, solution 2 is added to solution 1 with vigorous stirring. The obtained clear mixture (solution 3) is coated on flat substrates such as glass, silicon wafer, polyethylene terephthalate (PET),

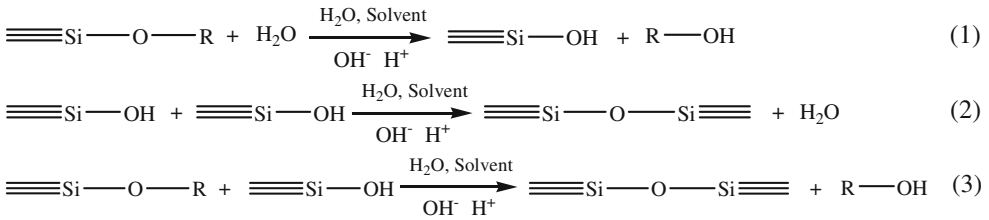

Scheme 1 The crosslinking reaction mechanism of STP to form 3D hybrid network

polypropylene (PP), or polytetrafluoroethylene (PTFE) sheets. Coating is obtained either by dipping the substrate in the solution or by casting the solution on the substrate and removing the excess solution with the aid of a sliding glass rod (doctor blade method), direct casting, or screen-printing method. After aging for more than 1 h at room temperature (RT), a transparent solid layer with adjustable thickness forms on the substrates. In order to allow for a homogeneous crosslinking and ensure full crosslink, the sample is placed in a polypropylene food box to achieve an equalizing solvent evaporation condition and the hydrolysis and condensation reaction. After aging for 24 h at room temperature, the hybrid is post-cured at 60 °C for 5 h in a memmert oven. For preparing those samples with higher thickness, e.g., 1 mm, the hybrid solution is cast into a PTFE-based mould with a piece of PTFE board as the substrate and another drilled piece on top as the baffle of the mould. Thus, moisture can penetrate from both top and intervals from the bottom, providing a better homogeneity. Other processing conditions are the same as described for the thin film preparation steps.

The hybrids were produced via a sol–gel process in dichloromethane (DCM), which is a good solvent for both STP and the titania precursor (TTIP). It is well known that titanium alkoxides are highly reactive toward nucleophiles and they can be easily hydrolyzed when exposed to moisture [37]. As there is sufficient amount of water in the humid air, in the sol–gel process there is no need to add additional water [38]. In order to improve the homogeneity of titania in the hybrid material network and to reduce the optical losses, the STP was diluted in DCM by 40 wt% and mixed with a same concentration of TTIP in DCM with different ratios. The sol–gel was then carefully applied to the substrates to form a homogeneous film. After applying the sol–gel to the substrate, it was placed in a polypropylene-based box in the fume hood to allow for an equalizing evaporation of the solvent.

Characterizations

We characterized the hybrids by Attenuated Total Reflection–Fourier Transform Infrared (ATR–FTIR) on a FTS 6000 (Bio-Rad, USA) Fourier transform infrared spectrometer. The thin film samples were cast onto a piece of silicon plate (1.5×1.5 cm^2). For each sample, 16 scans were performed. All such samples were dried overnight in desiccators over P_2O_5 before the FTIR analysis.

Tensile test was carried out on an Advanced Rheometric Expansion System (ARES) (TA instruments, USA). After the hybrids were cured on a smooth polypropylene (PP) substrate, the free-standing hybrid thin films were obtained by peeling them carefully from the PP substrate and then cut into small strips with the dimension near $40 \times 3 \times 0.1$ mm^3 (each was accurately confirmed by a caliper), and mounted onto the thin film tensile test fixture of ARES. The measurement was conducted at 25 °C with a 2000 g-cm transducer. The extension speed was 0.2 mm/s in a strain-controlled mode. In each condition, 12 specimens were measured and the data collected for analysis.

Thermogravimetric analysis (TGA) measurements were carried out on a Q5000 (TA instruments, USA) thermogravimetric analyzer. Temperature used was raised from 25 to 600 °C at 10 °C/min. Differential scanning calorimetry (DSC) measurements are carried out on a DSC-Q100 (TA instruments, USA), equipped with a liquid-nitrogen cooling system. The hybrid samples (about 6 mg) are subjected to three subsequent heating runs at 10 °C/min from -80 up to +100 °C. T_g values are taken at half-height of the glass transition heat capacity step. Both TGA and DSC experiments were carried out in nitrogen atmosphere.

The UV-blocking property of the hybrid films were characterized on a double beam scanning spectrometer, model Lambda 20 (Perkin-Elmer, USA) in the range 200–800 nm with a scan rate of 600 nm/min. Transparent quartz plate (500 μm in thickness) was used as the substrate on which a hybrid layer (~6 μm thick) was coated. Transmittance of the coated quartz square plate is measured with changing wavelength.

The surface morphology of the hybrids were characterized by the field emission scanning electron microscopy (FE-SEM) (JEOL 6700F, Japan). Before the SEM observation, 200 angstrom (in thickness) of gold was sputtered on the sample surface.

Radiographic images of the hybrids are recorded on a Cabinet X-ray system (Faxitron X-ray Corporation, USA).

22 keV, 4 mA/s and 11 cm sample to detector distance (Level 8). The thickness of the hybrid layer is about 1 mm.

Results and discussion

Figure 2 shows the FT-IR spectra of the hybrids with different titania content. These set of data were obtained from the hybrid samples on a piece of double side polished silicon wafer in transmission mode. Three bands located at 2970, 2930, and 2870 cm^{-1} correspond to the overlapping bands of the C–H stretches of the polyether carbohydrate [33]. Band at 1105 cm^{-1} corresponds to the C–O–C ether vibrations of the polypropylene oxide main chain [39, 40], while the one at 1375 cm^{-1} corresponds to the in plane bending of C–H from the polypropylene oxide main chain [39, 41]. The small peak at 1345 cm^{-1} is contributed by the CH_2 wagging, small peak at 1298 cm^{-1} is the CH_2 twisting, and the peak at 1014 cm^{-1} is the CH_2 rocking [42]. The peak at 1455 cm^{-1} is contributed by the tensile vibration of the C–O bond [43]. The spectra for titania-containing samples do not show the well-defined absorption bands typical of the crystalline titanium dioxide polymorphs (anatase, rutile, etc.). We only observe the spectrum curves in close agreement with the literature spectrum for completely amorphous TiO_2 [44]. The result is comprehensible, because of the room temperature (25 °C) and relatively short treatment time which are not expected to promote crystal phase formation [45, 46]. The most prominent features in the TiO_2 spectrum are: (a) the wide OH stretching region centered at 3300 cm^{-1} and spanning over 1000 cm^{-1}, where the vibrations of Ti–OH and of absorbed water appear; and (b) the broad absorption region ranging from 400 to 900 cm^{-1} that is typical Ti–O–Ti vibrations of amorphous titanium dioxide [47, 48]. The peak at 1650 cm^{-1} in the cured TTIP and the hybrid samples is due to the moisture absorbed from the air. The small peak at 1660 cm^{-1} in the control PEU (H-0) corresponds to the C=O vibration of the amide bond near the end group [49, 50]. The relatively low intensity of this peak is due to the minor content of this functional group relative to the high molecular weight.

The crosslinking of the hybrid is basically attributed to the ability of the silane-terminated group to condense with each other and condense with TTIP as well. In order to further investigate the chain mobility and phase behavior of the organic phases, we characterized the hybrids and the control plain PEU (H-0) by DSC. Figure 3 shows the analytic results. Comparing the data from the hybrids containing different titania content, there is only minor change (within 1 °C) of the glass transition temperature (T_g) of the PEU moiety. This suggests that in the hybrids, the existence of the inorganic moiety does not cause observable change to the mobility of the PEU main chain. This is also confirmed by the FT-IR analysis, which shows only overlap of the peaks of PEU and titania in the hybrids rather than any shifting or uprising of new peak.

A group of the samples were analyzed by the thermogravimetric analysis (TGA). Plain PEU (H-0) is also analyzed as a control. Figure 4 shows the TGA curves of the hybrid samples. The thermal residue weight percents of the samples at 600 °C are listed in the figure as pointed by the arrows. The plain PEU starts losing weight at about 280 °C, and is totally degraded when the temperature is

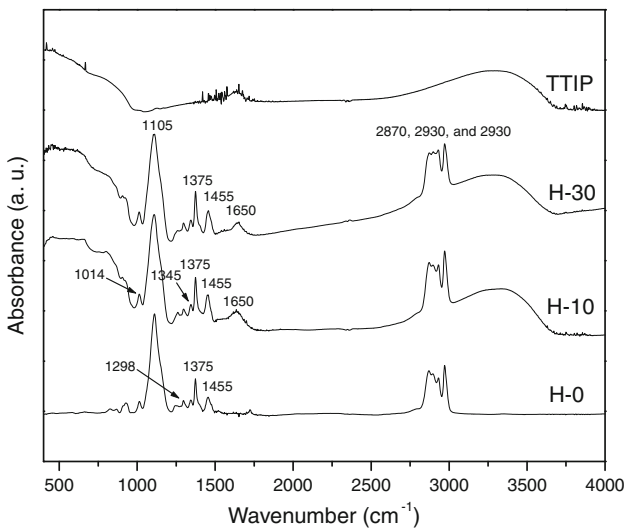

Fig. 2 FT-IR spectra of the hybrids: cured STP film (H-0); cured hybrid film with STP to TTIP 9:1 (H-10); cured hybrid film with STP to TTIP ratio 7:3 (H-30); and pure TTIP after cure

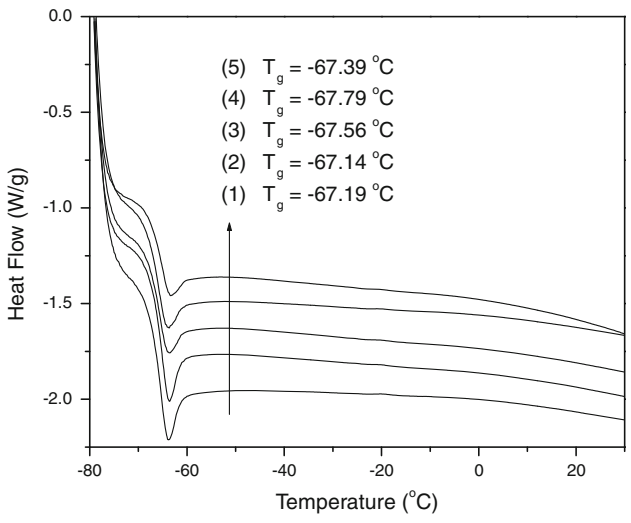

Fig. 3 DSC analysis of the hybrids with different titania contents. The *arrow* direction suggests the sequence number listed, which are: (1) H-0; (2) H-10; (3) H-20; (3) H-30; (4) H-40; and (5) H-50. Glass transition temperature (T_g) of each sample is listed

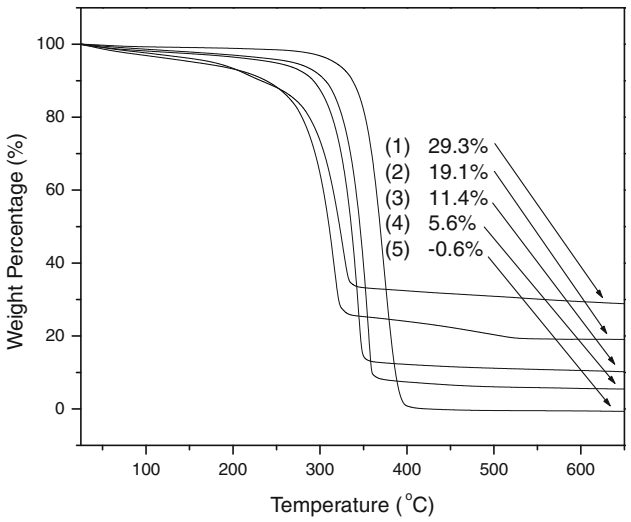

Fig. 4 TGA spectra of the hybrids performed in nitrogen atmosphere. (1) H-60; (2) H-50; (3) H-30; (4) H-15; and (5) H-0

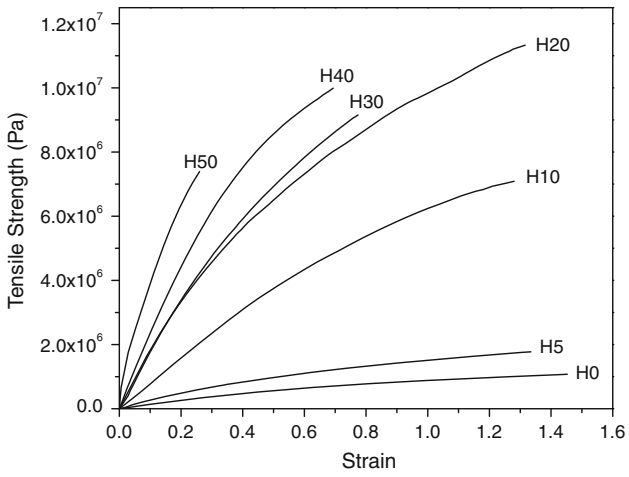

Fig. 5 Stress–strain curve of the hybrids containing different titania

above 400 °C, which led to negligible residue. The degradation of the hybrids starts at quite low temperatures, depending on the ratio between titania and PEU. When there is a higher content of TTIP, lower thermal stability of the hybrids than the pure PEU was observed. For example, at 200 °C, the hybrid sample with 60% TTIP loses 6.78% weight, hybrid sample with 50% TTIP loses 6.62% weight, hybrid sample with 30% TTIP loses 3.53% weight, hybrid sample with 15% TTIP loses 2.99% weight, and the plain PEU without TTIP loses 1.14% of weight. This difference might be related to degradation reactions involving titanium oxide, which is known as a catalyst, and also the different hydrolysis/condensation equilibrium reactions carried out in different conditions during the sol–gel process [23, 51–53]. When the temperature is higher than 600 °C, all organic parts are degraded; the remaining weight ratio after this heating scan are summarized in Table 1, which suggests the inorganic component of the samples.

Tensile test of the free-standing hybrid films were carried out with different titania content levels. The stress–strain curves of the tested samples are shown in Fig. 5. In spite of some scatters, the data here demonstrate the trend that with the increase of the titania content, there is an increasing Young's modulus and a decreasing elongation at break. The modulus of the hybrids is in the magnitude of $\sim 10^7$ Pa, which suggests a stiff elastomeric property. However, crack and shrinkage may become problems when the titania content is high. For example, when the TTIP content is as high as 60% (H-60), after curing, the tensile property of the hybrid film turns very unstable and the color of the sample gets cloudy (which may due to the uneven hydrolysis process and the increased size of the inorganic phase). Below that, the distribution of the inorganic phase is very homogeneous, as shown in Fig. 6, which is the surface morphology of four hybrid samples under SEM. Transmission electron microscopy with energy dispersive X-ray spectroscopy (EDS) result of the hybrid sample is elucidated in the supporting information. In these SEM image, nano-domains with the homogeneous size less than 10 nm can be observed; there is no observable large agglomeration of the nano-domains littered over the surface, which suggests excellent dispersion of the inorganic phase in the hybrids. Increasing the titania content will

Table 1 Thermal and mechanical properties of the hybrids

Sample name	TTIP content (%)	Weight residue at 600 °C (%)	Young's Modulus (MPa)	Elongation at break (%)	Tensile strength (MPa)
H-0	0	−0.6	1.45 ± 0.09	145.2 ± 7.69	1.07 ± 0.12
H-5	5	1.2	3.19 ± 0.25	133.5 ± 11.34	1.77 ± 0.14
H-10	10	3.5	7.99 ± 1.03	128.0 ± 14.05	7.09 ± 0.29
H-20	20	5.6	16.30 ± 2.31	131.6 ± 16.79	11.30 ± 0.84
H-30	30	11.4	23.74 ± 2.29	77.4 ± 10.83	9.99 ± 0.86
H-40	40	14.8	30.21 ± 4.18	69.3 ± 5.26	9.15 ± 1.25
H-50	50	19.1	67.11 ± 5.76	30.0 ± 4.77	7.39 ± 0.69

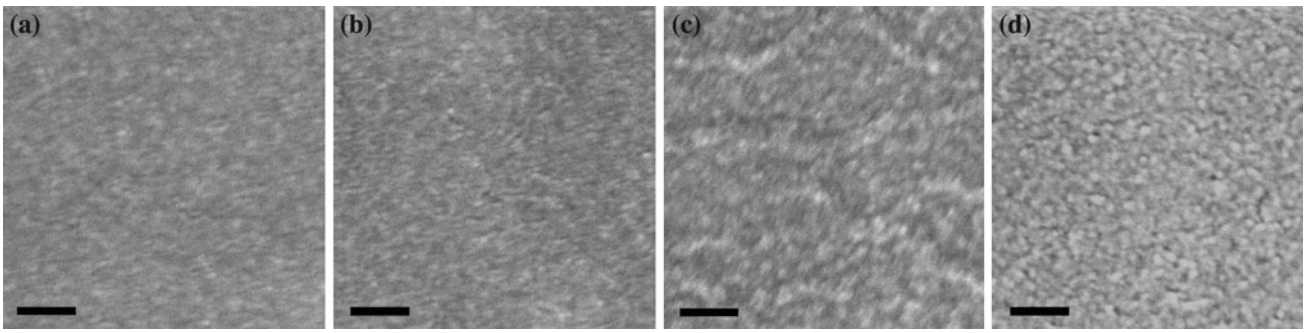

Fig. 6 SEM images of the surface of the hybrids. **a** H-5, **b** H-20, **c** H-40, and **d** H-50. (*Scale bar* 100 nm)

only result in larger sizes and more nano-domains and higher surface contrasts, while there is no observable dispersity problem. Since the interactions between the organic and inorganic phases are very weak (as confirmed by the DSC analysis and FTIR spectra), the nano-domains are the integrated inorganic parts.

We characterized the UV–vis transmission properties of the hybrid thin films (thickness $\sim$ 6 μm) in the form of thin layers coated on a piece of quartz plate (thickness $\sim$ 500 μm). Figure 7 shows the corresponding UV–vis transmittance spectra of three hybrids with different titania contents, namely, H-10, H-50, H-70, and the control H-0, coated on quartz. The thickness of each hybrid is controlled at 6 μm by screen printing. H-0 is the plain PEU-cast control sample, showing transmittance higher than 95% along the entire UVB/UVA range (280 nm $< \lambda <$ 400 nm) and the range of visible light (400 nm $< \lambda <$ 800 nm). In the same UVB/UVA range of light wavelength, hybrids H-10, H-50, and H-70 were able to cut off most of the UV radiation, but in the range of visible light wavelength, there is minor decrease of light transmittance as compared to H-0. The light transparency of the hybrid samples in visible range is mainly due to the nanometric dimension of titania domains that are not able to scatter radiation with wavelengths in this range [54]. UVB is in the range from 280 to 320 nm, which only covers a small fraction of the whole solar radiation. However, because of their high energy, they are responsible for most of the harmful effects of exposure to sunlight, such as skin cancers [55–57]. The synthesized hybrids are able to cut off a large part of the UVA spectrum, i.e., the UV-A2 range. In particular, for wavelengths lower than 345 nm, the transmitted radiation intensity is reduced down to below 50% (H-10), 37% (H-50), and 35% (H70). This suggests that a merely 6-μm-thick hybrid film can cut off most of the UV radiation with $\lambda <$ 330 nm.

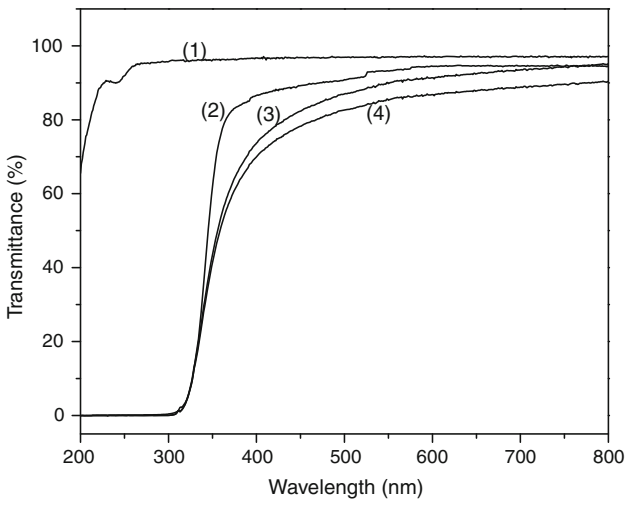

Fig. 7 UV–vis spectra of the quartz plates coated with the hybrid polymers containing different titania contents. (1) H-0; (2) H-10; (3) H-50; and (4) H-70

We further characterized the interaction between the hybrids and electromagnetic radiation. Figure 8a shows the photographic image of a piece of hybrid sample (H-40) with the thickness of 1 mm. The background of the sample bears some printed letters with the font size of 12 on a piece of A4 paper. In visible light, the hybrids are transparent solids, irrespective of inorganic phase content, which suggests that in the hybrids, titania form nanometric domains [54]. However, as shown in Fig. 8b, a clearly contrasted image is obtained when the material is investigated using a cabinet X-ray system. The shape of the sample is clearly discernible

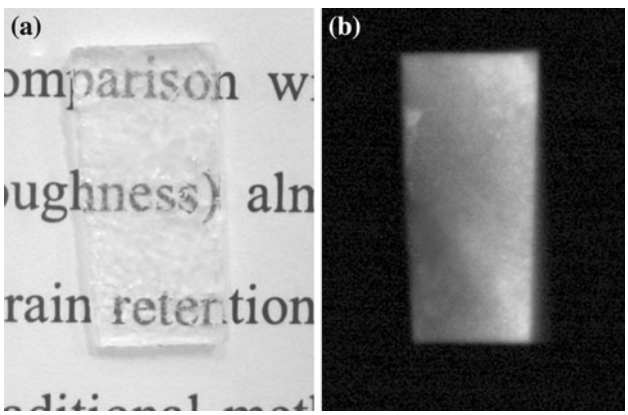

Fig. 8 **a** Photographic image and **b** radiographic image of the same transparent and radiopaque hybrid sample H-40

as a bright (radiopaque) area contrasting with the dark (radiotransparent) background. In the case of hybrids with lower titania content (pictures not shown), the radiographic picture of the hybrid is still very clear, although the contrast becomes weaker with decreasing the titania fraction.

Conclusion

This study demonstrates that the PEU-based hybrid materials with different titania content can easily be prepared at room temperature by moisture-curing method. Because of the weak interaction between the soft main chain and the titania phase, the hybrids exhibit excellent elastomeric and low Young's modulus. For example, the hybrid with 40% of titania precursor (H-40) can endure 69.3% of elastic deformation, thus rendering it suitable for applying to those elastic materials surfaces or surfaces which are susceptible to heat or having high coefficient of thermal expansion. In addition, these materials coated on transparent substrates show intrinsic optical transparency and the ability to completely block UVB and UVA radiations. These unique properties allow them to be used as molded materials, coatings, sealants, and adhesives in potential applications that require light weight, high resilience, and radiation blocking ability. This method can provide convenient solutions for new personal radiation protective equipments that are lighter and more flexible than the current lead-based protective gloves, face–shields, and joints for airtight clothing, etc.

Acknowledgements The authors acknowledge ITF GHP 009/06 from Hong Kong government for financial support, and Bayermaterialscience AU for providing the materials.

References

1. Backov R (2006) Soft Matter 2:452
2. Prouzet E, Ravaine S, Sanchez C, Backov R (2008) New J Chem 32:1284
3. Yang C, Liang GL, Xu KM, Gao P, Xu B (2009) J Mater Sci 44:1894. doi:10.1007/s10853-009-3247-8
4. Yang C, Gao P, Xu B (2009) J Mater Sci 44:469. doi:10.1007/s10853-008-3094-z
5. Zhai L, Cebeci FC, Cohen RE, Rubner MF (2004) Nano Lett 4:1349
6. Balazs AC, Emrick T, Russell TP (2006) Science 314:1107
7. Mascia L, Kioul A (1995) Polymer 36:3649
8. Jiang P, McFarland MJ (2004) J Am Chem Soc 126:13778
9. Ma ML, Hill RM (2006) Curr Opin Colloid Interface Sci 11:193
10. Wen JY, Wilkes GL (1996) Chem Mater 8:1667
11. Chattopadhyay DK, Raju K (2007) Prog Polym Sci 32:352
12. Wilkes GL, Orler B, Huang H (1985) Polymer Prepr 26:300
13. Sanchez C, Ribot F (1994) Gauthier-Villars, Paris, p 1007
14. Okada A, Usuki A (1995) Mater Sci Eng C 3:109
15. Du YJ, Damron M, Tang G, Zheng HX, Chu CJ, Osborne JH (2001) Prog Org Coat 41:226
16. Vendamme R, Onoue SY, Nakao A, Kunitake T (2006) Nat Mater 5:494
17. Gilman JW, Jackson CL, Morgan AB, Harris R, Manias E, Giannelis EP (2000) Chem Mater 12:1866
18. Porter D, Metcalfe E, Thomas MJK (2000) Fire Mater 24:45
19. Hsiue GH, Liu YL, Liao HH (2001) J Polym Sci A Polym Chem 39:986
20. Armes SP (1995) Polym News 20:233
21. Godovski DY (1995) Adv Polym Sci 119:78
22. Yabuta T, Tsuru K, Hayakawa S, Osaka A (2004) J Sol-Gel Sci Technol 31:273
23. Mazzocchetti L, Sandri S, Scandola M, Bergia A, Zuccheri G (2007) Biomacromolecules 8:672
24. Bashore TM (2004) Am Heart J 147:375
25. Tsuru K, Aburatani Y, Yabuta T, Hayakawa S, Ohtsuki C, Osaka A (2001) J Sol-Gel Sci Technol 21:89
26. Mazzocchetti L, Scandola M, Pollicino A (2008) Polymer 49:5215
27. Mazzocchetti L, Cortecchia E, Scandola M (2009) Appl Mater Interfaces 1:726
28. Smith DS, Scalo JM (2007) Los Alamos National Laboratory, Preprint Archive, Astrophysics, pp 1–8
29. Liao HT, Wu CS (2004) J Polym Sci B Polym Phys 42:4272
30. Mark JE (1996) Soc Plastics Eng Inc, p 2905
31. Kohjiya S, Ikeda Y (2000) Am Chemical Soc Inc, p 534
32. Mackenzie JD, Bescher E (2003) J Sol-Gel Sci Technol 27:7
33. Te′llez L, Rubio J, Rubio F, Morales E, Oteo JL (2004) Spectrosc Lett 37:11
34. Schapman F, Couvercelle JP, Bunel C (1998) Polymer 39:973
35. Matner M (2009) Asia Pac Coat J 22:20
36. Helminen A, Korhonen H, Seppala JV (2001) Polymer 42:3345
37. Livage J, Henry M, Sanchez C (1988) Prog Solid State Chem 18:259
38. Takahashi R, Takenaka S, Sato S, Sodesawa T, Ogura K, Nakanishi K (1998) J Chem Soc, Faraday Trans 94:3161
39. Srichatrapimuk VW, Cooper SL (1978) J Macromol Sci-Phys B15:267
40. Hummel DO, Ellinghorst G, Khatchatryan A, Stenzenberger HD (1979) Angew Makromol Chem 82:129
41. Tadokoro H, Umehara A, Murahashi S (1965) J Chem Phys 42:2807
42. Su YL, Wang J, Liu HZ (2002) Macromolecules 35:6426
43. Bahl OP, Manocha LM, Jain GC, Chari SS, Bhatia G (1979) J Sci Ind Res 38:537
44. Kickelbick G (2003) Prog Polym Sci 28:83
45. Li Y, White TJ, Lim SH (2004) J Solid State Chem 177:1372
46. Ge L, Xu M, Sun M, Fang H (2006) Mater Res Bull 41:1596
47. Velasco MJ, Rubio F, Rubio J, Oteo JL (1999) Thermochim Acta 326:91
48. McDevitt NT, Baun WL (1964) Spectrochim Acta 20:799
49. Jalsovszky G, Holly S, Hollosi M (1995) J Mol Struct 348:329
50. Chen S, Sui JJ, Chen L (2004) Colloid Polym Sci 283:66
51. Zeynalov EB, Allen NS (2006) Polym Degrad Stab 91:3390
52. Allen NS, Edge M, Ortega A, Sandoval G, Liauw CM, Verran J (2004) Polym Degrad Stab 85:927
53. Yang J, Zhang S, Liu X, Cao A (2003) Polym Degrad Stab 81:1
54. Caseri W (2000) Macromol Rapid Commun 21:705
55. Briviba K, Klotz LO, Sies H (1997) Biol Chem 378:1259
56. World Health Organization. Health effects of UV radiation http://www.who.int/uv/health/en/
57. Matsumura Y, Ananthaswamy HN (2004) Toxicol Appl Pharmacol 195:298